Pseudocapacitive Lithium Storage in TiO_2(B)

Markéta Zukalová,[†] Martin Kalbáč,[†] Ladislav Kavan,*[,†,‡] Ivan Exnar,[§] and Michael Graetzel[‡]

J. Heyrovský Institute of Physical Chemistry, Academy of Sciences of the Czech Republic, Dolejškova 3, CZ-18223 Prague 8, Czech Republic, Laboratory of Photonics and Interfaces, EPFL, Ecublens, CH-1015 Lausanne, Switzerland, and High Power Lithium, Park Scientifique, PSE-B, EPFL, Ecublens, CH-1015 Lausanne, Switzerland

Received October 6, 2004. Revised Manuscript Received December 16, 2004

Phase-pure TiO_2(B) with microfibrous morphology was prepared via a newly developed method from amorphous TiO_2. Cyclic voltammetry evidences that Li-insertion into TiO_2(B) is governed by a pseudocapacitive faradaic process, whose rate is not limited by solid-state diffusion of Li^+ in a broad interval of scan rates. This unusual behavior was discussed in terms of the crystal structure of the TiO_2(B) host, having freely accessible parallel channels for Li^+-transport perpendicular to the (010) face. The characteristic Li-insertion electrochemistry of TiO_2(B) allows re-interpretation of several previous reports, which did not consider explicitly this relation or the presence of TiO_2(B) in various TiO_2 materials of different origin.

Introduction

TiO_2(B) is a metastable monoclinic modification of titanium dioxide. It was first synthesized in 1980 by Marchand et al.[1,2] from a layered titanate $K_2Ti_4O_9$ via K^+/H^+ ion exchange followed by calcination.[1−3] Some other layered titanates, namely, $Na_2Ti_3O_7$ and $Cs_2Ti_5O_{11}$, also give TiO_2(B) upon ion exchange and thermal dehydratation.[4,5] The $H_2Ti_4O_9 \cdot H_2O$ can be exfoliated into nanosheets by tetrabutylammonium cations and further converted into oriented TiO_2(B) films.[6] Alternatively, $H_2Ti_4O_9 \cdot H_2O$ can be transformed to TiO_2(B) by solvothermal treatment.[7−9] The TiO_2(B) materials prepared from $H_2Ti_xO_{2x+1}$ ($x = 3-5$) are presumably all microcrystalline, the BET surface areas being 14−30.4 m^2/g.[2,10] Nanocrystalline TiO_2(B) (crystal size 5−10 nm) was first prepared by annealing of sol−gel derived SiO_2-TiO_2 amorphous film at 900 °C.[11] TiO_2(B) was also observed during ball milling of anatase.[12,13] (Note some mismatch in the notation of TiO_2(B) and the badelleyite-type TiO_2 ($P2_1/c$ space group) in ref 12). The "β-TiO_2" (apparently TiO_2(B)) was observed in titania films made by laser deposition.[14]

TiO_2(B)[15−18] and "monoclinic TiO_2" (apparently TiO_2(B))[8] were traced during the synthesis of titania nanotubes by hydrothermal treatment of TiO_2 in NaOH medium. This subject was pioneered by Kasuga et al.[19] in 1998, albeit "bundles of fibrous units" and TiO_2(B) were found in hydrothermally treated TiO_2/NaOH much earlier, too.[20] By tuning of the temperature and concentration of NaOH, either titanate nanotubes or TiO_2(B) nanowires were synthesized selectively.[18] The structure of hydrothermally grown nanotubes has been a subject of some confusion in the past, but recent studies point at the layered titanate, $H_2Ti_3O_7$, as the main constituent of these nanotubes.[17,18,21] There was an alternative suggestion that the hydrothermally grown titanate nanotubes are composed of orthorhombic lepidocrocite-like species, $H_xTi_{2-x/4}\square_{x/4}O_4 \cdot H_2O$ ($x \approx 0.7$, $\square$ = vacancy),[22] which transforms directly to anatase by heating.[22,23] However, this work was criticized by others,[17] and the sole presence of monoclinic titanates (trititanates) seems to explain the

* Corresponding author. E-mail: kavan@jh-inst.cas.cz.
† Academy of Sciences of the Czech Republic.
‡ Laboratory of Photonics and Interfaces.
§ High Power Lithium.

(1) Marchand, R.; Brohan, L.; Tournoux, M. *Mater. Res. Bull.* **1980**, *15*, 1129.
(2) Tournoux, M.; Marchand, R.; Brohan, L. *Prog. Solid State Chem.* **1986**, *17*, 33.
(3) Brohan, L.; Verbaere, A.; Tournoux, M.; Demazeau, G. *Mater. Res. Bull.* **1982**, *17*, 355.
(4) Feist, T. P.; Davies, P. K. *J. Solid State Chem.* **1992**, *101*, 275.
(5) Feist, T. P.; Mocarski, S. J.; Davies, P. K.; Jacobson, A. J.; Lewandowski, J. T. *Solid State Ionics* **1988**, *28−33*, 1338.
(6) Sugimoto, W.; Terabayashi, O.; Murakami, Y.; Takasu, Y. *J. Mater. Chem.* **2002**, *12*, 3814.
(7) Yin, S.; Uchida, S.; Fujishiro, Y.; Aki, M.; Sato, H. *J. Mater. Chem.* **1999**, *9*, 1191.
(8) Yin, S.; Fujishiro, Y.; Wu, J.; Aki, M.; Sato, T. *J. Mater. Proc. Technol.* **2003**, *137*, 45.
(9) Yin, S.; Wu, J.; Aki, M.; Sato, T. *Int. J. Inorg. Mater.* **2000**, *2*, 325.
(10) Wallenberg, L. R.; Sanati, M.; Andersson, A. *Microsc. Microanal. Microstruct.* **1990**, *1*, 357.
(11) Kogure, T.; Umezawa, T.; Kotani, Y.; Matsuda, A.; Tatsumisago, M.; Minami, T. *J. Am. Ceram. Soc.* **1999**, *82*, 3248.
(12) Bose, P.; Pradhan, S. K.; Sen, S. *Mater. Chem. Phys.* **2003**, *80*, 73.
(13) Sen, S.; Ram, M. L.; Roy, S.; Sarkar, B. K. *J. Mater. Res.* **1999**, *14*, 841.
(14) Lackner, J. M.; Waldhauser, W.; Ebner, R.; Major, B.; Schoberl, T. *Surf. Coat. Technol.* **2004**, *180−181*, 585.
(15) Gao, X.; Zhu, H.; Pan, G.; Ye, S.; Lan, Y.; Wu, F.; Song, D. *J. Phys. Chem. B* **2004**, *108*, 2868.
(16) Sasaki, T.; Komatsu, Y.; Fujiki, Y. *Chem. Mater.* **1992**, *4*, 894.
(17) Suzuki, Y.; Yoshikawa, S. *J. Mater. Res.* **2004**, *19*, 982.
(18) Armstrong, A. R.; Armstrong, G.; Canales, J.; Bruce, P. G. *Angew. Chem., Int. Ed.* **2004**, *43*, 2286.
(19) Kasuga, T.; Hiramatsu, M.; Hoson, A.; Sekino, T.; Niihara, K. *Langmuir* **1998**, *14*, 3160.
(20) Nishizawa, H.; Aoki, Y. *J. Solid State Chem.* **1985**, *56*, 158.
(21) Chen, Q.; Du, G. H.; Zhang, S.; Peng, L. M. *Acta Crystallogr., Sect. B* **2002**, *58*, 587.
(22) Ma, R.; Bando, Y.; Sasaki, T. *Chem. Phys. Lett.* **2003**, *380*, 577.
(23) Fukuda, K.; Sasaki, T.; Watanabe, M.; Nakai, I.; Inaba, K.; Omote, K. *Cryst. Growth Des.* **2003**, *3*, 281.

10.1021/cm048249t CCC: $30.25
Published on Web 02/08/2005

hydrothermal synthesis of nanotubes adequately.[17,24] Since the $H_2Ti_3O_7$ can be thermally dehydrated to TiO_2(B),[4,5,17] the existence of TiO_2(B) nanotubes is supported, too.[17]

Banfield et al.[25] first found TiO_2(B) in nature. Its crystal structure was determined by Marchand et al.[1] (Note an error in ref 1, where the TiO_2(B) was confused with $K_2Ti_8O_{17}$). The structure was further refined by theoretical methods[26] and by X-ray[5] and neutron diffraction.[4] TiO_2(B) has monoclinic unit cell (space group $C2/m$) with $a = 1.21787$ nm, $b = 0.37412$ nm, $c = 0.65249$ nm, and $\beta = 107.054°$.[4] The structure is isotypic to that of Na_xTiO_2 (bronze), $x \cong 0.2$, where the name "TiO_2(B)" comes from.[27] (This name was, however, historically generated in a different way, first for VO_2(B)[28] and other isomorphous oxides including TiO_2(B)).[29] The same crystal structure is also represented by the mineral $Na_2Fe_2Ti_6O_{16}$ (freudenbergite).[30] Hence, TiO_2(B) can equally be called "freudenbergite modification of TiO_2", but this notation is not common. The structure of TiO_2(B) is characterized by two edge-sharing TiO_6 octahedra which are linked to the neighboring doublet of octahedra by corners. The density of TiO_2(B) is 3.64−3.76 g/cm^3[3,2,11,25] hence, it is smaller than that of anatase, rutile, or brookite.

The electronic structure of TiO_2(B) was calculated by Nuspl et al.[31] TiO_2(B) is an n-type semiconductor with a band gap of 3−3.22 eV,[9,32] which is similar to rutile and anatase. Consequently, TiO_2(B) shows photoanodic[32] and photocatalytic[8,9] activity in UV light. The photocatalytic activity may be even superior to that of Degussa P25.[8,9] Because of its open structure, TiO_2(B) accommodates hydrogen via electrochemical reduction of inserted protons, and this hydrogen can be extracted photoelectrochemically in visible light.[32]

TiO_2(B) also accommodates Li^+ to form Li_xTiO_2(B). The insertion coefficient x was 0.75−0.85 by the reaction with *n*-butyl-lithium and 0.5−0.75 by electrochemistry.[2,29,33−35] The electrochemical reversibility of lithium insertion was, reportedly, not very good.[2] Recently, high electrochemical capacity ($x = 0.82$, i.e., 275 mAh/g) was reported for hydrothermally grown TiO_2(B) nanowires.[18] A comparative theoretical study of Li-insertion into anatase and TiO_2(B) points at beneficial properties of the latter.[31] The TiO_2(B) lattice has parallel infinite channels, in which Li^+ can be accommodated, without any significant distortion of the structure.[31] This paper aims at deeper understanding of the Li insertion into TiO_2(B). It will allow rationalization of some previous reports,[15,36−40] in which the interaction of Li with TiO_2(B) was probably overlooked.

Experimental Section

Materials. The precursor, X-ray amorphous TiO_2, was prepared by precipitation of the aqueous solution of K_2TiF_6 (Aldrich) with ammonium hydroxide solution (25 wt %, Fluka). The product was washed with H_2O and dried, $S_{BET} = 584$ m^2/g. Alternatively, the amorphous TiO_2 ($S_{BET} = 518$ m^2/g) was prepared by hydrolysis of titanium isopropoxide at 0 °C as described elsewhere.[41]

Sample A. 3.5 g of amorphous TiO_2 was autoclaved in 100 mL of 10 M NaOH at 250 °C for 48 h and then washed with H_2O and autoclaved in 0.1 M HNO_3 at 200 °C for 2.5 h. The dried sample was then calcined at 500 °C for 1 h. The surface area of the product was 34.7 m^2/g.

Sample B. 10 g of amorphous TiO_2 was mixed with 7.78 g of Cs_2CO_3 (Aldrich) and mortared carefully. The mixture was then decarbonated at 800 °C for 4 h, mortared again, and annealed at 800 °C in a crucible with a tight lid for 24 h, twice, with grinding at the interval. The product was then mortared and ion-exchanged with 1 M HCl (100 mL per 1 g of product) for 4 × 24 h at vigorous stirring with the fresh acid exchanged every 24 h. The dried sample was finally calcined at 500 °C for 1 h. The product contained <10 ppm K (according to ICP analysis) and its surface area was $S_{BET} = 29.5$ m^2/g.

Sample C. This material was prepared according to the original synthetic protocol of TiO_2(B).[1] An intimate mixture of 20 g KNO_3 (Aldrich) and 31.6 g of TiO_2 (Bayer, PKP04090) was annealed at 1000 °C for 2 days. The product was mortared and hydrolyzed with 0.4 N HNO_3 (100 mL of HNO_3 per 1 g of product) for 3 days at vigorous stirring with the fresh acid every 24 h. The sample was dried in air at ambient temperature and then under vacuum overnight and was calcined at 500 °C for 30 min. The final product contained 120 ppm K (according to ICP analysis), and its surface area was $S_{BET} = 9.9$ m^2/g.

Preparation of Electrodes. Powder sample was dispersed in aqueous medium into viscous paste according to the previously developed methods.[42−44] The powder (0.3 g) was mixed under stirring or gentle mortaring with 0.8 mL of 10% aqueous solution of acetylacetone. Subsequently, 0.8 mL of 4% aqueous solution of hydroxypropylcellulose (Aldrich, MW 100 000) was added, and finally 0.4 mL of 10% aqueous solution of Triton-X100 (Fluka) was also added. Before use, the prepared slurry was homogenized by stirring. If the slurry was too viscous, it was further diluted by water. Titanium grid (5 × 15 mm, Goodfellow) was used as the electrode support. Electrodes were prepared by dip-coating, and the coated area was ca. 5 × 5 mm^2. The prepared electrodes were

(24) Sun, X.; Li, Y. *Chem. Eur. J.* **2003**, *9*, 2229.
(25) Banfield, J.; Veblen, D.; Smith, D. *Am. Mineral.* **1991**, *76*, 343.
(26) Catlow, C. R. A.; Cormack, A. N.; Theobald, F. *Acta Crystallogr.* **1984**, *B40*, 195.
(27) Andersson, S.; Wadsley, A. D. *Acta Crystallogr.* **1962**, *15*, 194.
(28) Theobald, F.; Cabala, R.; Bernard, J. *J. Solid State Chem.* **1975**, *17*, 431.
(29) Zachau-Christiansen, B.; West, K.; Jacobsen, T.; Skaarup, S. *Solid State Ionics* **1992**, *53−56*, 364.
(30) Ishiguro, T.; Tanaka, K.; Marumo, F.; Ismail, M. G. M. U.; Hirano, S.; Somiya, S. *Acta Crystallogr.* **1978**, *B34*, 255.
(31) Nuspl, G.; Yoshizawa, K.; Yamabe, T. *J. Mater. Chem.* **1997**, *7*, 2529.
(32) Betz, G.; Tributsch, H.; Marchand, R. *J. Appl. Electrochem.* **1984**, *14*, 315.
(33) Kawamura, H.; Muranishi, Y.; Miura, T.; Kishi, T. *Denki Kagaku* **1991**, *59*, 766.
(34) Zachau-Christiansen, B.; West, K.; Jacobsen, T.; Atlung, S. *Solid State Ionics* **1988**, *28−30*, 1176.
(35) Brohan, L.; Marchand, R. *Solid State Ionics* **1993**, *9−10*, 419.
(36) Kavan, L.; Rathousky, J.; Grätzel, M.; Shklover, V.; Zukal, A. *J. Phys. Chem. B* **2000**, *104*, 12012.
(37) Kavan, L.; Rathousky, J.; Grätzel, M.; Shklover, V.; Zukal, A. *Microporous Mesoporous Mater.* **2001**, *44−45*, 653.
(38) Kavan, L.; Kalbac, M.; Zukalova, M.; Exnar, I.; Lorenzen, V.; Nesper, R.; Grätzel, M. *Chem. Mater.* **2004**, *16*, 477.
(39) Kavan, L.; Zukalova, M.; Kalbac, M.; Grätzel, M. *J. Electrochem. Soc.* **2004**, *151*, A1301.
(40) Zhou, Y.; Cao, L.; Zhang, F.; He, B.; Li, H. *J. Electrochem. Soc.* **2003**, *150*, A1246.
(41) Zhang, H.; Finnegan, M.; Banfield, J. F. *Nano Lett.* **2001**, *1*, 81.
(42) Kavan, L.; O'Regan, B.; Kay, A.; Grätzel, M. *J. Electroanal. Chem.* **1993**, *346*, 291.
(43) Nazeeruddin, M. K.; Kay, A.; Rodicio, I.; Humphry-Baker, R.; Mueller, E.; Liska, P.; Vlachopolous, N.; Grätzel, M. *J. Am. Chem. Soc.* **1993**, *115*, 6382.
(44) Kavan, L.; Grätzel, M.; Rathousky, J.; Zukal, A. *J. Electrochem. Soc.* **1996**, *143*, 394.

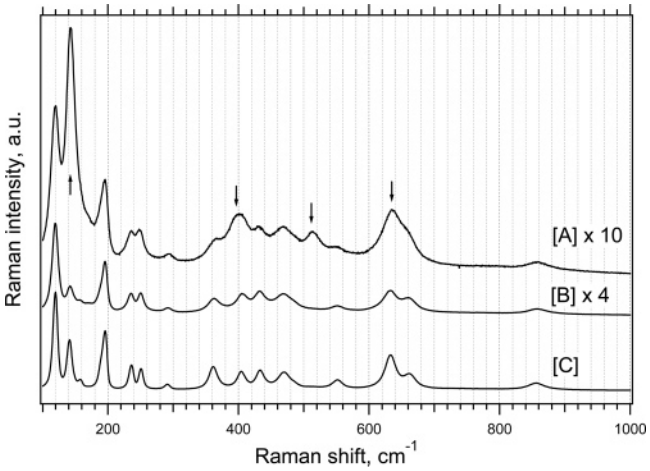

Figure 1. Raman spectra of the prepared materials A−C. Spectra B and C are assignable to monoclinic TiO_2(B), spectrum A also shows the anatase peaks (marked by arrows) in addition to TiO_2(B). The Raman intensities of samples A and B are multiplied by a factor of 10 and 4, respectively. Spectra are offset for clarity.

dried in air and finally calcined in air at 450 °C for 30 min. The amount of active electrode material was between 0.2 and 0.7 mg. Blank experiments confirmed that a bare Ti grid had negligible electrochemical charge capacity compared to that of the active material. Alternatively, the slurry was also deposited on a sheet of conducting glass (F-doped SnO_2, TEC 8 from Libbey−Owens−Ford, 8 Ω/square) using a doctor-blading technique.[44] The sheet of conducting glass had dimensions: $3 \times 5 \times 0.3$ cm^3. A Scotch-tape at both edges of the support (0.5 cm) defined the film thickness and left part of the support uncovered for electrical contact. The film was finally calcined for 30 min in air at 450 °C. After cooling to room temperature, the sheet was cut into 10 electrodes 1.5×1 cm^2 in size; the geometric area of the TiO_2 film was 1×1 cm^2. To improve the mechanical properties, the electrode was sometimes pressed by stainless steel blocks (5000 N/cm^2).

Methods. Electrochemical measurements were carried out in a one-compartment cell using an Autolab Pgstat-30 (Ecochemie) controlled by the GPES-4 software. The reference and auxiliary electrodes were from Li metal, hence, potentials are referred to the Li/Li^+ (1M) reference electrode. $LiN(CF_3SO_2)_2$ (Fluorad HQ 115 from 3M) was dried at 130 °C/1 mPa. Ethylene carbonate (EC) and 1,2-dimethoxyethane (DME) were dried over the 4A molecular sieve (Union Carbide). The electrolyte solution, 1 M $LiN(CF_3SO_2)_2$ + EC/DME (1/1 by volume), contained 15−40 ppm H_2O as determined by Karl Fischer titration (Metrohm 684 coulometer). All operations were carried out under argon in a glovebox. The BET surface areas of the prepared materials were determined from nitrogen adsorption isotherms at 77 K (ASAP 2010, Micromeritics). Raman spectra were excited by an Ar^+ laser at 2.41 eV (Innova 305, Coherent) and recorded on a T-64000 spectrometer (Instruments, SA). Scanning electron microscopy images were obtained using JEOL JSM-03 microscope. Powder X-ray diffraction (XRD) was studied on a Siemens D-5000 diffractometer using CuKα radiation. Transmission electron microscopy (TEM) images were obtained on Tecnai F30 microscope with 300 keV field emission electron gun.

Results and Discussion

Figure 1 shows Raman spectra of the prepared materials. Sample A is, apparently, a mixture of anatase and TiO_2(B), but the spectra of samples B and C can be assigned to TiO_2(B)[4,5,18] only. The mixture of TiO_2(B) with anatase[5,15,18] or rutile[17] is a typical product of calcination of hydrothermally grown layered titanates (such as $H_2Ti_3O_7$).[15,18] The same holds for calcination products from $H_2Ti_xO_{2x+1}$ (x = 3, 4, 5) obtained by an ordinary solid-state reaction protocol.[2,4−6,16] The structure of $H_2Ti_xO_{2x+1}$ is characterized by corrugated ribbons containing 3, 4, or 5 TiO_6 octahedra in flat sections.[4] Since TiO_2(B) has only two edge-sharing TiO_6 octahedra in the corresponding sections, the transformation of $H_2Ti_xO_{2x+1}$ ($x = 3-5$) into TiO_2(B) is, apparently, not topotactic, but it is promoted by the kinks in the precursor's structure.[4,10]

Some authors did not explicitly mention the formation of TiO_2(B) during calcination of titanate nanotubes ($H_2Ti_xO_{2x+1}$). The obvious reasons are two: either the temperature was high enough to recrystallize TiO_2(B) into anatase and rutile or the TiO_2(B) phase was simply overlooked. The later problem was articulated by Kogure et al.:[11] TiO_2(B) may easily be unnoticed in a mixture with large concentration of anatase because of an overlap of the main diagnostic XRD peaks, especially in nanocrystalline materials with broad diffraction maxima (cf. Figure 2). Raman spectroscopy is a convenient analytic tool (cf. Figures 1 and 2), since TiO_2(B) can be unambiguously distinguished from anatase and other TiO_2 phases. (Note ref 15 for the opposite conclusion, which, however, may look questionable, if we inspect the actual Raman spectrum presented in ref 15.)

The diffractogram of sample B (Figure 2) matches well the pattern of monoclinic TiO_2(B) from JCPD PDF No.35-0088. Hence, its phase purity is confirmed both by XRD and Raman spectroscopy (cf. Figure 1). The XRD of sample C (Figure 2) is similar but exhibits an extra peak at 2 theta = 11.8°, which indicates some amount of unconverted hydrogen titanates, such as tetratitanate ($H_2Ti_4O_9 \cdot 0.25\ H_2O$) or octatitanate ($H_2Ti_8O_{17} \cdot 0.4H_2O$). The latter species is formed from tetratitanate at 200−300 °C,[45] and its presence is supported also by the Li-insertion voltammogram (see below). The classical solid-state synthesis of $K_2Ti_4O_9$ precursor may give side products $K_2Ti_6O_{13}$ and $K_2Ti_2O_5$.[46,47]

The formation of pure TiO_2(B) in sample B (Figures 1, 2) is surprising. The employed synthetic protocol should, actually, lead to the orthorhombic lepidocrocite-like protonic titanate, $H_xTi_{2-x/4}\square_{x/4}O_4$. This species is characterized by ideally flat sheets of edge-sharing TiO_6 octahedra,[48−50] which convert directly into anatase,[22,23] without the intermediate crystallization of TiO_2(B). We have explored this discrepancy, and it turned out that the occurrence of TiO_2(B) is crucially dependent on the TiO_2 precursor in the synthesis of the first intermediate, that is, the Cs-titanate. Nanocrystalline anatase TiO_2 (Bayer) provided mixtures of TiO_2(B) and anatase or pure anatase in the final product, but the syntheses starting from amorphous TiO_2 (see Experimental section) lead, unexpectedly, to pure TiO_2(B).

(45) Suzuki, S.; Miyayama, M. *Key Eng. Mater.* **2003**, *248*, 151.
(46) Zaremba, T.; Hadrys, A. *J. Mater. Sci.* **2004**, *39*, 4561.
(47) Krogh Andersen, E.; Krogh Andersen, I. G.; Skou, E. *Solid State Ionics* **1988**, *27*, 181.
(48) Sasaki, T.; Nakano, S.; Yamauchi, S.; Watanabe, M. *Chem. Mater.* **1997**, *9*, 602.
(49) Sasaki, T.; Watanabe, M. *J. Am. Chem. Soc.* **1998**, *120*, 4682.
(50) Choy, J. H.; Lee, H. C.; Jung, H.; Kim, H.; Boo, H. *Chem. Mater.* **2002**, *14*, 2486.

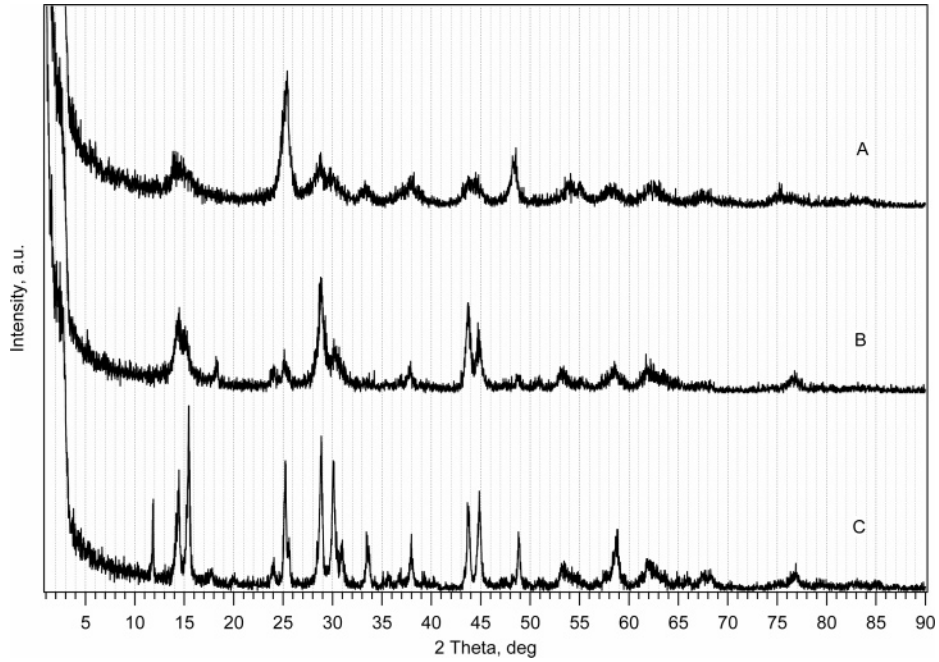

Figure 2. X-ray diffractograms of samples A−C. The plots are offset for clarity.

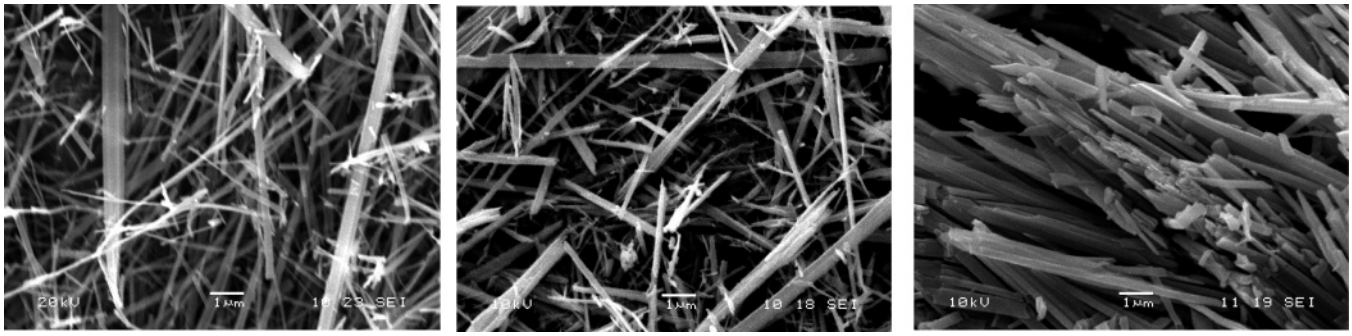

Figure 3. Scanning electron microscopy images of samples A−C (from left to right). Scale bars correspond to 1 μm.

Apparently, structures other than orthorhombic $Cs_xTi_{2-x/4}\square_{x/4}O_4$ ($x \approx 0.7$) may play a role in this case. For instance, if we assume the $Cs_2Ti_5O_{11}$ as an intermediate Cs-titanate, the formation of pure TiO_2(B) is smoothly explained.[4] Also, another flat structure, $Cs_2Ti_6O_{13}$, is partly transferable to TiO_2(B).[4] The particular reactions giving either orthorhombic lepidocrocite or monoclinic pentatitanate are only distinguished by a small difference in the stoichiometry of reactants: Cs/Ti = 0.4 for pentatitanate and Cs/Ti = 0.38 for lepidocrocite, respectively. Hence, the usual product is a mixture of both materials.[16]

All samples A−C show characteristic fibrous texture as indicated by scanning electron microscopy (SEM) (Figure 3). The fibers of sample C are of larger size, which is also mirrored by narrower XRD peaks, smaller BET area, and intense Raman peaks of this sample (see above). Generally, the fibers of TiO_2(B) are of polycrystalline,[18] mosaic[2] texture, but single crystalline[10] fibers can be observed, too. The mosaic and single crystalline fibers tend to be oriented parallel to the *b*-axis of the TiO_2(B) lattice.[2,10] This is also documented by a high-resolution TEM image of our sample B (Figure 4). The same orientation exists in $K_2Ti_4O_9$, which is a common precursor of TiO_2(B).[10]

Figure 5 shows schematically the TiO_2(B) structure in the (010) projection. This scheme is somewhat idealized, as the

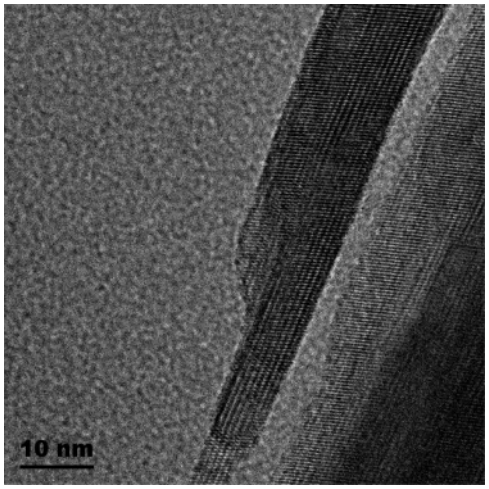

Figure 4. Transmission electron microscopy image of the sample B; scale bar corresponds to 10 nm.

TiO_6 octahedra are slightly distorted in the real structure. However, it clearly depicts characteristic parallel channels running perpendicular to the (010) face. Since microfibrous particles of TiO_2(B) materials tend to be oriented along the *b*-axis[10,18] (cf. Figure 4), these channels also run parallel to the microfiber axis. The cross section of a channel is comparable to the size of "missing" TiO_6 octahedron in the

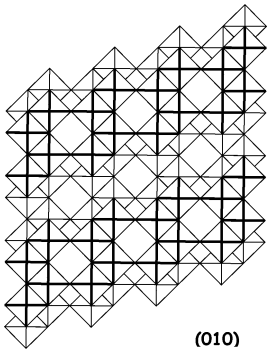

Figure 5. Projection of the idealized structure of TiO_2 (B) perpendicular to the (010) face.

structure (Figure 5), hence, the channel is large enough to accommodate Li^+ ions and to allow their easy transport along the fiber axis. This seems to be the key for understanding of the fast (pseudocapacitive) Li-storage in this material (see below).

Figure 6 displays cyclic voltammograms of Li-insertion into the samples A−C. The voltammogram of sample A exhibits a pair of cathodic/anodic peaks at 1.75 and 1.95 V (formal potential 1.85 V), which are characteristic for Li-insertion into anatase lattice.[38,39,44,51−56] We have previously denoted this pair of peaks as "A-peaks".[38] In addition to that, the voltammogram shows two pairs of peaks with formal potentials of 1.52 and 1.59 V vs Li/Li^+, respectively, denoted S1 and S2, respectively.[38] The notation came from our earlier assumption that these S-peaks could be assigned to the surface-confined process in titania nanosheets[38] or in "amorphous phase".[36,37] However, this assumption needs revision in view of the new facts accumulated in this paper (see below).

The sole features assignable to S-peaks occur in both samples B and C, which are almost pure TiO_2(B). This generates a logical conclusion that the S-peaks are, actually, signatures of TiO_2(B) phase. The Li-storage capacity (Li/Ti $= x$) at the slowest voltammetric scan (0.1 mV/s) was 0.53 (sample A), 0.68 (sample B), and 0.47 (sample C). These capacities are comparable to those reported for galvanostatic charging of bulk TiO_2(B) ($x = 0.5$)[29,34] but smaller than the values obtained for galvanostatic charging of TiO_2(B) nanowires ($x = 0.82$).[18] Also from theoretical arguments, the Li-insertion beyond $x = 0.5$ becomes rather difficult.[31] Sample C sometimes exhibited poorly reproducible electrochemistry. On the other hand, samples A and B gave well-defined voltammograms, which did not change significantly during tens of voltammetric cycles. The broad and overlapping S-peaks in sample C are reminiscent of the Li-insertion behavior of monoclinic octatitanate, $H_2Ti_8O_{17}$, which has just one pair of broad peaks in this potential region.[28] The octatitanate is formed by heating of the TiO_2(B) precursor, $H_2Ti_4O_9$, at moderate temperature, 200 °C, and we may recall that the XRD of sample C confirms the presence of unconverted titanates (see above). The titanates in sample C seem to influence mechanical properties of the electrode. The material is poorly workable during the electrode fabrication because of its hardness. Consequently, the films are less uniform and sensitive to mechanical cracking upon electrochemical treatment.

Figure 7 demonstrates the behavior of S-peaks in the phase-pure sample B at varying scan rates. The peak currents were normalized with respect to the peak current at the slowest scan (0.1 mV/s) and plotted against the scan rate (inset in Figure 7). Apparently, the currents scale with the first power of scan rate, which is characteristic for capacitive charging:

$$i = \mathrm{d}Q/\mathrm{d}t = C\,\mathrm{d}E/\mathrm{d}t = C\upsilon \qquad (1)$$

Q is the voltammetric charge, C is capacitance, and $\mathrm{d}E/\mathrm{d}t$ is the scan rate, υ. However, sole capacitive double-layer charging (eq 1) should give a featureless voltammogram (ideally rectangle assuming C invariant of potential). The peak structure with small peak-to-peak splitting (ca. 50−100 mV at $\upsilon = 0.1$ mV/s) points at a surface-confined charge-transfer process, which can be considered faradaic pseudocapacitance. The found Li-storage capacity ($x \approx 0.5$−0.7) considerably exceeds the "ordinary" capacity of the TiO_2 surface assuming solely the double layer plus the faradaic pseudocapacitance of surface states.[51] Consequently, this behavior is specific for the TiO_2(B), and we may suggest that its open structure with freely accessible channels[31] is responsible for the fast Li-charging of a TiO_2(B) crystal.

The different mechanism of Li-storage in TiO_2(B) and anatase is explicitly demonstrated at sample A which is a mixture of both phases (Figure 8A, B). The plot of peak currents against the scan rate is shown in Figure 8B. To analyze this dependence in a broader interval of υ, we selected here the cathodic S-peaks and anodic A-peaks, which are better resolved at faster charging (cf. also Figure 7). (However, the general conclusions are equally valid for both cathodic and anodic peaks.) Apparently, the A-peaks scale with square root of the scan rate, υ, as it is expected for diffusion-controlled irreversible process:[56,57]

$$|i| = 0.4958nFAc\,(D\alpha nF\upsilon/RT)^{1/2} \qquad (2)$$

where n is the number of electrons, A is the electrode area, c is the maximum concentration of Li^+ (or Ti^{3+}) in the accumulation layer ($c = 0.024$ mol/cm^3 for $x = 0.5$), D is the diffusion coefficient, and the other symbols have their usual meaning. Figure 8B confirms that this dependence can be fitted to experimental points for $\upsilon <\approx 2$ mV/s. (For higher scan rates, the fit shows systematic deviation due to uncompensated iR drop of the cell.) The behavior described by eq 2 is typical for Li-insertion into ordinary anatase lattice.[36−39,44,51−56] The $i \approx \upsilon^{1/2}$ dependence was even found

(51) Kavan, L.; Kratochvilová, K.; Grätzel, M. *J. Electroanal. Chem.* **1995**, *394*, 93.
(52) Van de Krol, R.; Goossens, A.; Meulenkamp, E. A. *J. Electrochem. Soc.* **1999**, *146*, 3150.
(53) Hengerer, R.; Kavan, L.; Krtil, P.; Grätzel, M. *J. Electrochem. Soc.* **2000**, *147*, 1467.
(54) Kavan, L.; Attia, A.; Lenzmann, F.; Elder, S. H.; Grätzel, M. *J. Electrochem. Soc.* **2000**, *147*, 2897.
(55) Kavan, L.; Grätzel, M.; Gilbert, S. E.; Klemenz, C.; Scheel, H. J. *J. Am. Chem. Soc.* **1996**, *118*, 6716.
(56) Lindström, H.; Södergen, S.; Solbrand, A.; Rensmo, H.; Hjelm, J.; Hagfeldt, A.; Lindquist, S. E. *J. Phys. Chem. B* **1997**, *101*, 7717.
(57) Van de Krol, R.; Goossens, A.; Schoonman, J. *J. Phys. Chem. B* **1999**, *103*, 7151.

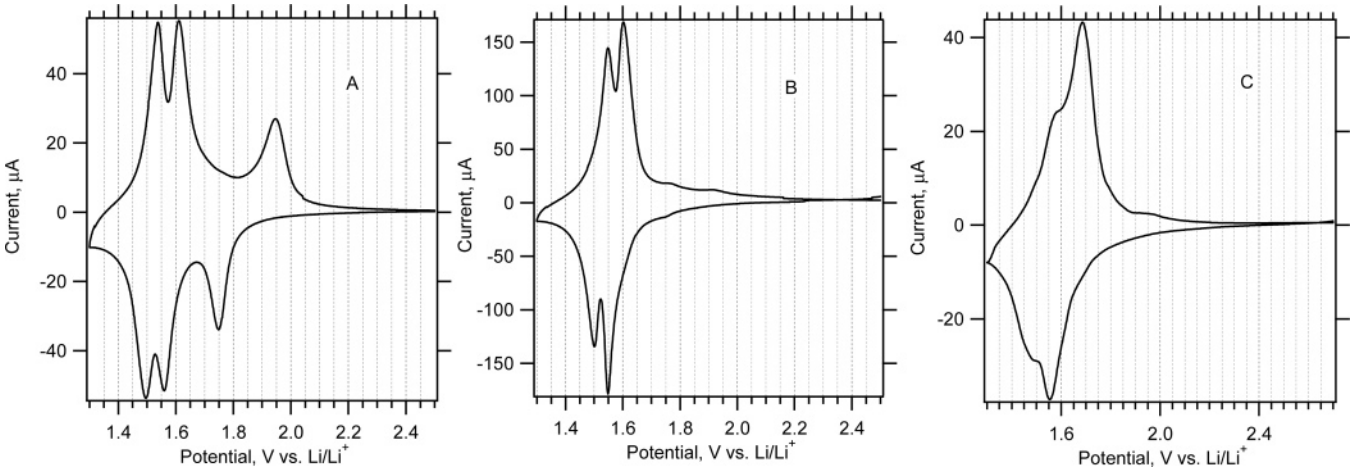

Figure 6. Cyclic voltammograms of samples A (chart A), B (chart B), and C (chart C) in 1M $LiN(CF_3SO_2)_2$ + EC/DME (1/1, v/v); scan rate 0.1 mV/s. The mass of active material was different for each particular electrode in charts A−C.

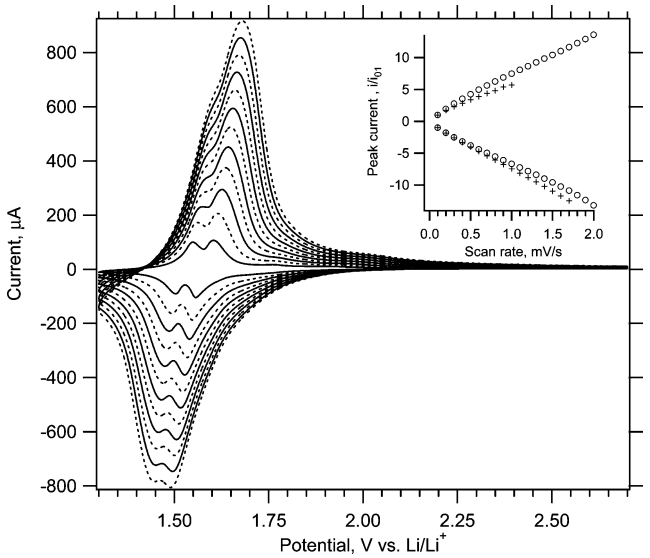

Figure 7. Cyclic voltammograms of sample B in 1M $LiN(CF_3SO_2)_2$ + EC/DME (1/1, v/v); scan rate 0.1−1.2 mV/s (in 0.1 mV/s steps for plots from bottom to top). Inset displays the normalized peak current, i/i_{01}, where i_{01} is the peak current at the slowest scan (0.1 mV/s) and i is the peak current at the actual scan rate. Circles and crosses denote two individual S-peaks.

for Li-insertion into titania nanosheets derived from lepidocrocite-like titanate.[58]

The conclusion that sample A accommodates Li either via the insertion into the anatase lattice or via the surface-confined pseudocapacitive process matches, phenomenologically, the conclusion of our previous works on similar materials.[36−39] Here we suggest, as new interpretation, that the S-peaks are assignable to TiO_2(B). The TiO_2(B) phase was, actually, traced in certain samples made by hydrothermal growth in ref 38 (see Supporting Information to ref 38). The apparent link between S-peak and TiO_2(B) was overlooked also by other authors, who had studied virtually identical systems.[15,40] Gao et al.[15] observed unstable features similar to S-peaks in a material declared as TiO_2(B) + anatase mixture, but these features were unclearly interpreted as "discrete phase or imperfections of the TiO_2 nanorod lattice". Analogously, the voltammogram of Zhou et al.[40] showed weak S-peaks, but they were not commented, nor was the presence of TiO_2(B) mentioned in this paper. Weak S-peaks were traceable also in TiO_2 made by galvanostatic oxidative hydrolysis of $TiCl_3$,[39] but TiO_2(B) was again unnoticed.

Strong S-peaks were detected in mesoscopic TiO_2 films made by templating with amphiphilic triblock copolymers (Pluronic).[36,37] The TiO_2(B) phase was not considered,[36,37] despite the fact that one Raman spectrum shown in ref 37 brought clear (but uncommented) evidence for TiO_2(B) in the Pluronic-templated material. Also, other papers dealing with Pluronic-templating[59−61] did not mention the TiO_2(B) phase, either. To rationalize this discrepancy, we have reproduced the relevant syntheses[36,37] and varied systematically the conditions (concentration of the precursor's solution, time of aging, temperature, heating program, etc.). The appearance of TiO_2(B)/S-peaks was poorly reproducible, and we failed to demonstrate pure TiO_2(B) in this way. In accord with other reports on Pluronic-templating,[36,37,59−61] the main crystalline phase was anatase, sometimes also brookite was observed,[60] while these crystals are embedded in a matrix of amorphous titania. The growth of metastable TiO_2(B) phase during the templating protocol requires, apparently, special conditions, which are not yet precisely known. The situation is reminiscent of the unexpected detection of TiO_2(B) during calcination of sol−gel derived SiO_2−TiO_2 amorphous film at 900 °C.[11] Also in this case, the matrix of amorphous silica promoted the growth and unusual stability of TiO_2(B).[11]

Li-insertion into pure TiO_2(B) was previously studied mostly by galvanostatic chronopotentiometry.[18,29,34] This technique is less suitable for the detection and analysis of the S-peaks. Nevertheless, derivation of the chronopotentiometric curve and plotting of dx/dE versus E shows clearly two pairs of cathodic/anodic peaks at ca. 1.6 and 1.5 V,[34] which is in remarkable accord with our voltammograms (Figures 6−8). Zachau-Christiansen et al.[34] have suggested

(58) Sakai, N.; Ebina, T.; Takada, K.; Sasaki, T. *J. Am. Chem. Soc.* **2004**, *126*, 5851.

(59) Yang, P.; Zhao, D.; Margolese, D. I.; Chmelka, B. F.; Stucky, G. D. *Chem. Mater.* **1999**, *11*, 2813.

(60) Crepaldi, E. L.; Soler-Illia, G. J. A. A.; Grosso, D.; Cagnol, F.; Ribot, F.; Sanchez, C. *J. Am. Chem. Soc.* **2003**, *125*, 9770.

(61) Choi, S. Y.; Mamak, M.; Coombs, N.; Chopra, N.; Ozin, A. *Adv. Funct. Mater.* **2004**, *14*, 335.

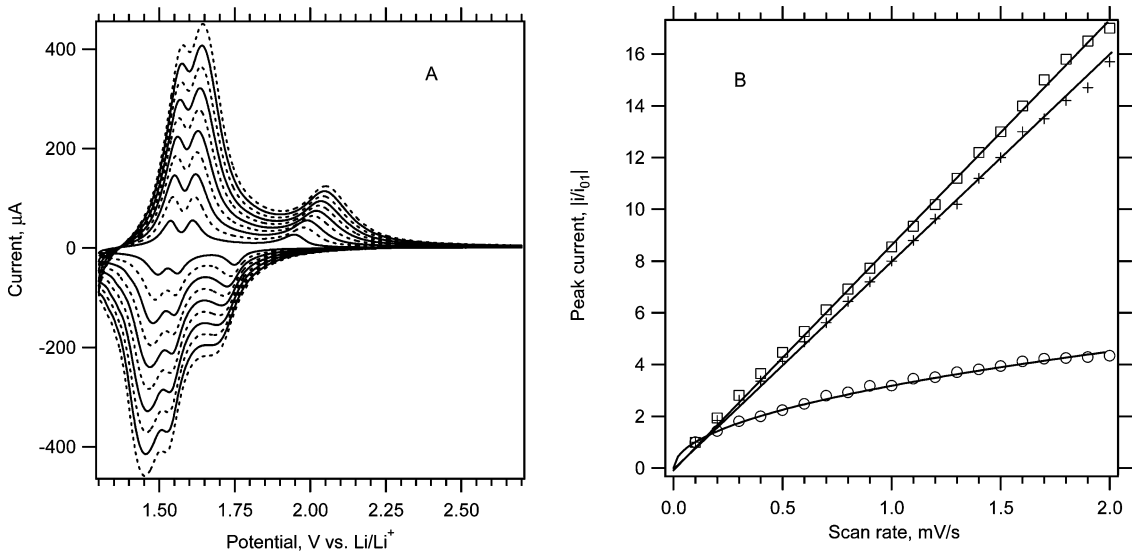

Figure 8. (A) Cyclic voltammograms of sample A in 1M $LiN(CF_3SO_2)_2$ + EC/DME (1/1, v/v); scan rate 0.1−1.0 mV/s (in 0.1 mV/s steps for plots from bottom to top). (B) Normalized peak current, i/i_{01}, where i_{01} is the peak current at the slowest scan (0.1 mV/s). Circles: anodic peak at ca. 2 V; crosses: cathodic peak at ca. 1.6 V, squares: cathodic peak at ca. 1.5 V.

that these peaks indicate two ordered superstructures with $x = 0.33$ and $x = 0.5$. Also, our S-peak at 1.6 V tends to be stronger than the S-peak at 1.5 V (Figures 6−8), that is, the first formed superstructure (at 1.6 V) is more populated by Li than the superstructure formed at 1.5 V. However, none of the previous electrochemical studies on TiO_2(B)[2,15,18,29,31,34,35] mentioned the pseudocapacitive nature of charging.

The fact that Li is accommodated in TiO_2(B) via pseudocapacitive process recalls the idea of fast transport of Li^+ in parallel channels of the TiO_2(B) lattice.[31] The channels run perpendicular to (010) face of TiO_2(B) (cf. Figure 5). This face is abundant at the cross section of typical microfibrous particles of TiO_2(B) (cf. Figures 3−5 and discussion thereof). During electrochemical insertion, Li^+ ions interact with the whole surface of a fibrous particle. Hence, Li^+ ions, perhaps, penetrate into the bulk fiber also in radial direction and not only through the cross section of a fiber (channel). Assuming the channels conduct rapidly Li^+ ions inside a particle, the rate-determining process is the primary interfacial Li^+-transfer at the fiber surface. This would provide rational for the surface-confined, pseudocapacitive process, controlling the overall kinetics. Such a "macroscopic" model highlights the role of fiber surface. The latter is dominated by the (100) and (001) faces, but the (010) face is negligibly engaged in the Li^+-transfer, occurring just at the tip of a fiber. We may further speculate that the two S-peaks reflect different energy barriers for Li^+ transfer at the (100) and (001) faces, which is quite reminiscent of the Li-insertion anisotropy in anatase.[53]

Alternatively, we may discuss these issues at "microscopic" level, too. Assuming that neither the intrachannel Li^+-transport nor the interfacial Li^+-transfer are rate-determining, the overall kinetics might still be controlled by trapping of Li^+ at certain sites at the inner wall of a channel. Also, this would mimic the pseudocapacitive faradaic process. Since all channels in the TiO_2(B) lattice are structurally equivalent,[31] there should be two distinct superstructures in Li_xTiO_2(B), which would give rise to the two S-peaks. Although $Li_{0.5}TiO_2$(B) is assumed to have crystallographically equivalent sites occupied by Li^+, there are further vacant sites up to the stoichiometry of $LiTiO_2$(B).[31] All these sites are quasi-octahedral with a coordination number of 5 (LiO_5),[31,35] while two kinds of these sites are detectable by ^{7}Li NMR.[35] If these two sites are occupied at $x < 0.5$, the occurrence of S-peaks-doublet is rationalized, too.

At this stage, we are unable to distinguish between the macroscopic and microscopic models and elucidate the origin of S-peaks unambiguously. However, our interpretation generates a logical question, whether the pseudocapacitive Li-storage would be observable also in other structures with one-dimensional parallel channels, such as ramsdellite[62] and hollandite[63] forms of TiO_2. This question was not yet clearly addressed, either. The TiO_2 (ramsdellite) accommodates Li reversibly up to ca. 200 mAh/g,[62] but the TiO_2 (hollandite) shows poor Li-storage electrochemistry despite the very wide open channels in the lattice.[63] Apparently, the good pseudocapacitive performance is observed only in structures having both the open pathways for bulk Li-transport and proper sites for reversible Li-anchoring in close vicinity of these pathways. TiO_2(B) seems to offer both these features simultaneously.

Conclusions

New synthetic protocol was elaborated giving phase-pure TiO_2(B) with microfibrous morphology. Amorphous TiO_2 was converted via a solid-state reaction with Cs_2CO_3 followed by the Cs^+/H^+ ion exchange and final calcination. Compared to traditional syntheses from $K_2Ti_4O_9$, the new product had finer fibers and also exhibited better electrochemical performance and stability.

Li-insertion electrochemistry of TiO_2(B) is basically different from that of anatase. Accommodation of Li in the

(62) Gover, R. K. B.; Tolchard, J. R.; Tukamoto, H.; Murai, T.; Irvine, J. T. S. *J. Electrochem. Soc.* **1999**, *146*, 4348.
(63) Noailles, L. D.; Johnson, C. S.; Vaughey, J. T.; Thackeray, M. M. *J. Power Sources* **1999**, *81−82*, 259.

TiO_2(B) lattice manifests itself by two pairs of peaks in cyclic voltammogram with formal potentials of ca. 1.5 and 1.6 V (S-peaks). Whereas the kinetics of lithium storage in anatase is controlled by solid-state diffusion of Li^+, the TiO_2(B) host accommodates lithium by a pseudocapacitive faradaic process, which is not controlled by diffusion at comparable conditions.

Pseudocapacitive electrochemical storage of Li^+ in TiO_2(B) fibers was discussed in terms of crystal structure of the host. The key effect seems to be fast Li^+ transport in the open channels running parallel to the *b*-axis. This direction coincides, usually, with the fiber axis in TiO_2(B) materials of fibrous morphology. The rate-limiting process might be either the Li^+-transport through the surface of fibrous particles or reversible trapping of Li^+ ions at the inner wall of the channel. This subject, apparently, requires further studies.

The assignment of S-peak to TiO_2(B) asks for reinterpretation of several previous reports, which did not consider this relation or the presence of TiO_2(B). The detection of S-peaks represents a sensitive and easy analytical tool for identification of this phase in titania materials. It turns out that the TiO_2(B) is present in a broad palette of TiO_2 materials of various origin.

Acknowledgment. This work was supported by the Grant Agency of the Czech Republic (contract No. 203/03/0824) and by the EC-COST Action D14/0002/99. We are grateful to Dr. L. Brabec (JHIPC) for SEM measurements. ICP analyses were carried out by Ecochem, a.s. Prague. M.Z. also thanks the Grant Agency of the Czech Republic for financial support (through grant No. 203/03/H140).

CM048249T